ELSEVIER

Journal of Wind Engineering
and Industrial Aerodynamics 69–71 (1997) 189–201

JOURNAL OF wind engineering AND industrial aerodynamics

Numerical simulation of unsteady low-Reynolds number flow around rectangular cylinders at incidence

A. Sohankar[a], C. Norberg[b], L. Davidson[a,*]

[a] *Thermo and Fluid Dynamics, Chalmers University of Technology, S-412 96 Göteborg, Sweden*
[b] *Division of Heat Transfer, Lund Institute of Technology, Box 118, S-221 00 Lund, Sweden*

Abstract

Calculations of unsteady two-dimensional-flow around rectangular cylinders at incidence are presented. The Reynolds numbers are low ($\leqslant 200$), so that the flow presumably is laminar. The results are in reasonable agreement with the indeed scarce experimental data available at these low Reynolds numbers. An incompressible SIMPLEC code is used employing non-staggered grid arrangement. A third-order QUICK scheme is used for the convective terms. The time discretization is implicit and a second-order Crank–Nicolson scheme is employed. The influence of the cylinder side ratio ($B/A = 1$–4) at various angles of incidence ($\alpha = 0°$–$90°$) is investigated. A number of quantities such as Strouhal number, drag, lift, and moment coefficients are calculated. Time sequences of fully saturated flow are also provided.

1. Introduction

For many decades, the flow around slender cylindrical bluff bodies has been the subject of intense research, mostly by experiments but recently also by using numerical simulation. This type of flow is of relevance for many practical applications, e.g. vortex flowmeters, bridges, towers, masts and wires. From an engineering point of view, the prediction of wall pressures, forces, moments and dominating wake frequencies is of great importance. In addition, the study of unsteady slender bluff-body wakes can be motivated from a purely fundamental basis. In many cases, engineering structures have a rectangular or near-rectangular cross section, e.g. beams, fences and other building construction details. Owing to the considerable effort involved in taking unsteady measurements and calculations, our knowledge of unsteady flow around cylinders having non-circular cross sections is limited, especially for rectangular cylinders at incidence.

* Corresponding author. E-mail: lada@tfd.chalmers.se.

0167-6105/97/$17.00
PII S0167-6105(97)00154-2

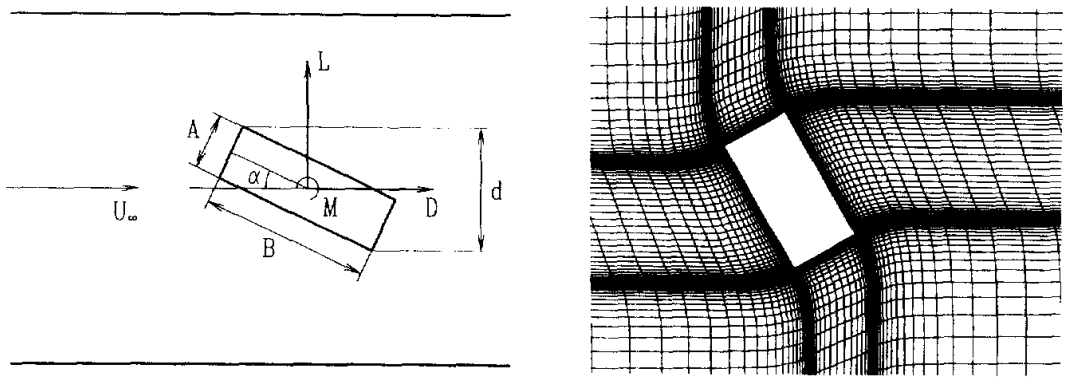

Fig. 1. Flow configuration (left) and close-up of grid near cylinder (right). $N_b = 40$.

The main objective of the present study is to provide reliable results from simulations of the flow around fixed, i.e. non-vibrating, rectangular cylinders at incidence. Special emphasis is put on factors such as time and spatial resolution, grid dependence, and the influence of domain size. Apart from providing general flow features on laminar vortex-shedding flows, the results to be presented will be of relevance as input for engineering models on vortex-induced sound and vibration.

The flow configuration is depicted in Fig. 1. A fixed two-dimensional rectangular cylinder with a side ratio B/A, where B is the longest side of the cylinder, is exposed, at some angle of incidence α, to a constant free stream velocity U_∞. Incompressible flow with constant fluid properties is assumed. The Reynolds number is defined as $\mathrm{Re} = U_\infty d/\nu$, where d is the projected width of the cylinder in the streamwise direction, $d = A\cos\alpha + B\sin\alpha$ ($0^\circ \leqslant \alpha \leqslant 90^\circ$). All geometrical lengths are scaled with d. The scaling with d also applies to the Strouhal number, $\mathrm{St} = f_S d/U_\infty$, where f_S is the shedding frequency, and for all forces and moment coefficients. The vertical distance between the upper and lower walls, H, defines the solid blockage of the confined flow. For all results in this paper, $H = 20$, corresponding to a solid blockage of 5%. Velocities are scaled with U_∞ and physical times with d/U_∞. Pitching moment M is referred to the geometrical center with positive values in the clockwise direction. The origin of coordinates is placed at geometrical center with drag force D positive in the x-direction and lift L positive in the y-direction, see Fig. 1. The base suction coefficient, $-C_{pb}$, was calculated from the pressure at the intersection of the cylinder and the base centerline.

In turbulent flows, i.e. for $\mathrm{Re} > 300$ approximately, there is a considerable amount of experimental data gathered at angles of incidence $\alpha = 0^\circ$, 90°, i.e. with one side of the cylinder facing the flow, see e.g. Refs. [1,2]. In such investigations the results usually are presented with h/d as a parameter, where h is the projected length of the cylinder. Experimental investigations on the effect of flow incidence can be found in Ref. [2] and references cited therein. In presumed laminar flow, i.e. for $\mathrm{Re} \leqslant 200$ approximately, simulations of 2D-flows around rectangular cylinders are presented in Refs. [3–15]. Among these, only Refs. [3,4,7,11] present results for non-square sections. Studies on the effects on flow incidence are exceptional – the only one covering arbitrary flow angles is that of Zaki et al. [13] in which results for the square cylinder at $\mathrm{Re} = 5$–50 are presented.

In previous numerical work by the authors [15], for the square cylinder at zero incidence, influence of time step, distribution of grid points, size of cells adjacent to the body, solid blockage and upstream and downstream extents of the calculation domain are thoroughly investigated (Re = 100). For this flow configuration, it is indicated that the relatively strong sensitivity to numerical parameters and solid blockage might explain the disparity of numerical results presented in the literature. Influence of Reynolds number (Re = 45–250) at 5% blockage is also presented. In agreement with simulations in Ref. [9], the onset of vortex shedding is found to occur in between Re = 50 and 55.

At Reynolds numbers relevant to this study, i.e. Re $\leqslant$ 200, the only experimental results available in the open literature seem to be in Refs. [3,4,16,17].

2. Numerical details

The flow is assumed to be two-dimensional and unsteady. An incompressible SIMPLEC finite-volume code is used employing a non-staggered grid arrangement. The scheme is implicit in time, and a Crank–Nicolson scheme which is of second order has been used for convective and diffusive terms; the pressure is treated fully implicitly. The convective terms are discretized using the third-order QUICK differencing scheme whereas the diffusive terms are discretized using central differences, which means second order accuracy. More details of the code, equations, etc. are described in Ref. [18].

At the inlet, which is located X_u units upstream of the most upstream corner of the cylinder, a uniform flow is assumed ($U = 1$, $V = 0$). At the outlet, which is located X_d units downstream of the most downstream corner, a zero gradient boundary condition for both U and V is used. It is important to emphasize that if the outlet is selected sufficiently far from the body, this Neumann type of boundary condition at outlet works well [15,12]. No-slip conditions are prescribed at the body surfaces. At the upper and lower boundaries symmetry conditions simulating a frictionless wall are used. The second normal derivative for the pressure is set to zero at all boundaries.

The time-marching simulations are started with the fluid at rest, after which the inlet velocity, within a few time steps, is increased smoothly to unity. The time step Δt was kept constant during all simulations. During the iterative sequence, convergence is assessed at the end of each iteration on the basis of the residual sources criterion which compares the sum of the absolute residual source over all the control volumes in the computation field, for each finite-volume equation. The residuals for the continuity and momentum are normalized with the incoming mass flux and momentum flux in the x-direction, respectively. The convergence criterion is set to 0.001.

Outside a region from the body which extends 5 units upstream, downstream and sideways, the grid distribution was made uniform with a constant cell size Δ. The distance from the cylinder surface to the nearest grid point defines the cell size δ. The hyperbolic tangent function was used for stretching the cell sizes between these limits, see Fig. 1. The number of nodes which are distributed over one unit length of

a cylinder surface is denoted by N_b. Except otherwise stated, the following numerical parameters were used (standard case): $\Delta t = 1/40$, $\delta = 0.004$, $\Delta = 0.5$, $N_b = 20$, $X_u = 10$, $X_d = 26$.

All quantities presented in this paper apply to the fully saturated flow condition. The statistics, i.e. time mean and RMS values, are based upon integrations during an integer number of the shedding period determined from the signal of fluctuating lift.

3. Results and discussion

An extensive investigation of the influence of various computation parameters as well as physical parameters such as Reynolds number, cylinder side ratio and angle of incidence was performed. In the fully saturated state, i.e. at physical times when memory effects of the starting process are negligible, many useful physical quantities were computed, for example, dominating wake frequency, mean and RMS values for various wall pressures, lift, drag and moments, respectively. In addition, for some selected cases, sequences of flow patterns within this saturated state are presented.

3.1. Influence of numerical parameters

All sensitivity studies on the influence of numerical parameters were carried out for the square cylinder, $B/A = 1$. The results are compiled in Tables 1 and 2.

A numerical error bar in the field of computational fluid dynamics (CFD) has been proposed by Karniadakis [19]. However, the identification and quantification of specific numerical errors may be very difficult, especially for time-dependent computations, non-uniform grids and complex geometries. Nevertheless, as suggested in Ref. [19], the error bar in calculations of vortex shedding flows may be divided into four parts: temporal and spatial errors, and errors due to computational domain size and boundary conditions.

Considering the influence of numerical parameters in vortex shedding flow simulations, the RMS lift coefficient is perhaps the best overall indicator. When using only the Strouhal number and/or the mean drag coefficient some of these effects do not

Table 1
Square cylinder at zero incidence, Re = 200: refinement study at $\Delta = 0.5$

n	Δt	Grid	δ	X_u	X_d	N_b	St	C_D	C_{D_p}	$C_{L'}$
1	1/40	126 × 96	0.004	10	26	20	0.167	1.439	1.480	0.227
2	1/40	120 × 88	0.008	10	26	20	0.165	1.442	1.481	0.243
3	1/80	126 × 96	0.004	10	26	20	0.168	1.438	1.479	0.234
4	1/40	145 × 96	0.004	20	26	20	0.165	1.419	1.458	0.221
5	1/40	180 × 96	0.004	20	40	20	0.165	1.415	1.455	0.227
6	1/40	127 × 96	0.002	10	26	20	0.167	1.427	1.469	0.199
7	1/80	127 × 96	0.002	10	26	20	0.168	1.433	1.476	0.214
8	1/40	146 × 114	0.004	10	26	40	0.163	1.462	1.504	0.265

Table 2
Square cylinder at incidence: effect of spatial resolution

n	Re	α	Grid	Δ	N_b	St	C_D	C_{D_p}	$C_{L'}$
1	100	0°	126 × 96	0.50	20	0.147	1.464	1.418	0.138
2	100	0°	191 × 141	0.30	20	0.146	1.477	1.433	0.156
3	200	0°	226 × 164	0.25	20	0.158	1.443	1.485	0.303
4	200	0°	348 × 224	0.20	30	0.149	1.445	1.488	0.360
5	200	20°	122 × 90	0.50	20	0.196	1.761	1.641	0.664
6	200	20°	185 × 135	0.30	20	0.196	1.796	1.675	0.707
7	200	45°	120 × 88	0.50	20	0.205	1.944	1.731	0.729
8	200	45°	182 × 133	0.30	20	0.204	2.022	1.798	0.790

show up correctly [15]. In Table 1, in which only cases at a far-field resolution of $\Delta = 0.5$ are considered, all values of St, C_D and C_{D_p} (the mean pressure drag coefficient) are within $\pm$ 2% whereas the variation in $C_{L'}$ is within $\pm$ 14%. Compared to the standard set of parameters, i.e. case 1 in Table 1, a doubling in the upstream extent X_u and a subsequent increase in the downstream extent X_d from 26 to 40 units (cases 4 and 5) only resulted in variations within a few percent, in accordance with the findings at Re = 100 [15]. When considering a smooth discharge of vortices with minimum upstream effects, the present outlet boundary condition with zero streamwise gradients for the velocity components (Neumann condition) is not the optimum choice. However, as also demonstrated in Ref. [15], a downstream extent greater than about 25 diameters is sufficient, at least for these low Reynolds numbers and with this outlet condition. To further validate the present results, we investigated the effects of changing the outlet boundary condition into a Sommerfelt radiation condition. In our recent investigation [20] it is shown that the necessary downstream extent of the domain then can be significantly reduced (down to about 10 units). When the outlet was placed sufficiently far downstream, the global results from simulations using the Neumann condition were virtually indistinguishable from results using the Sommerfelt condition [20]. Thus, as the blockage was kept constant at 5%, the errors due to computational domain size and boundary conditions can be regarded as very small (within a few percent).

Keeping other parameters constant at standard values, the separate influences of time step Δt and near-body resolution δ are small but somewhat difficult to interpret. At constant Re, the ratio $\Delta t/\delta$ is a measure on the maximum Courant number, which for high accuracy and physical realization in convective regions should be kept as small as possible, i.e. the temporal and spatial errors are coupled [21]. However, based on the assumption that the present time steps and the δ taken separately are sufficiently low for physical realization it seems that the major source of computational error is related to parameters Δ and N_b, i.e. to the maximum cell sizes in the field. When comparing case 4 in Table 2, which has $\Delta = 0.25$ and $N_b = 30$ with otherwise standard parameters, with the standard case at Re = 200, there is actually a 59% increase in the RMS lift! However, the influence of maximum cell sizes is much less at Re = 100, see Table 2. It also appears that cases with one side facing the flow

are the ones which are most sensitive to variations in Δ and N_b. The distribution of grid points along the body surface, as determined by δ, N_b and the used stretching function, and its relation to the far-field resolution and the stretched region around the body needs further investigation. Also, the relevance of the maximum Courant number in these simulations of low-Reynolds number shedding flows is an issue which will be investigated in the future. To sum this up, it is evident that the present standard case simulations were not independent of the grid. Nevertheless, they are believed to be good enough for showing up reasonable correct influences of physical parameters, to be presented in the following sections. The refinement cases will provide some guidance for the extent of the numerical error bar.

3.2. *Square cylinder at zero incidence*

A comparison between the present simulations and the results of others for the Strouhal number and mean drag coefficient are provided in Fig. 2. It needs to be

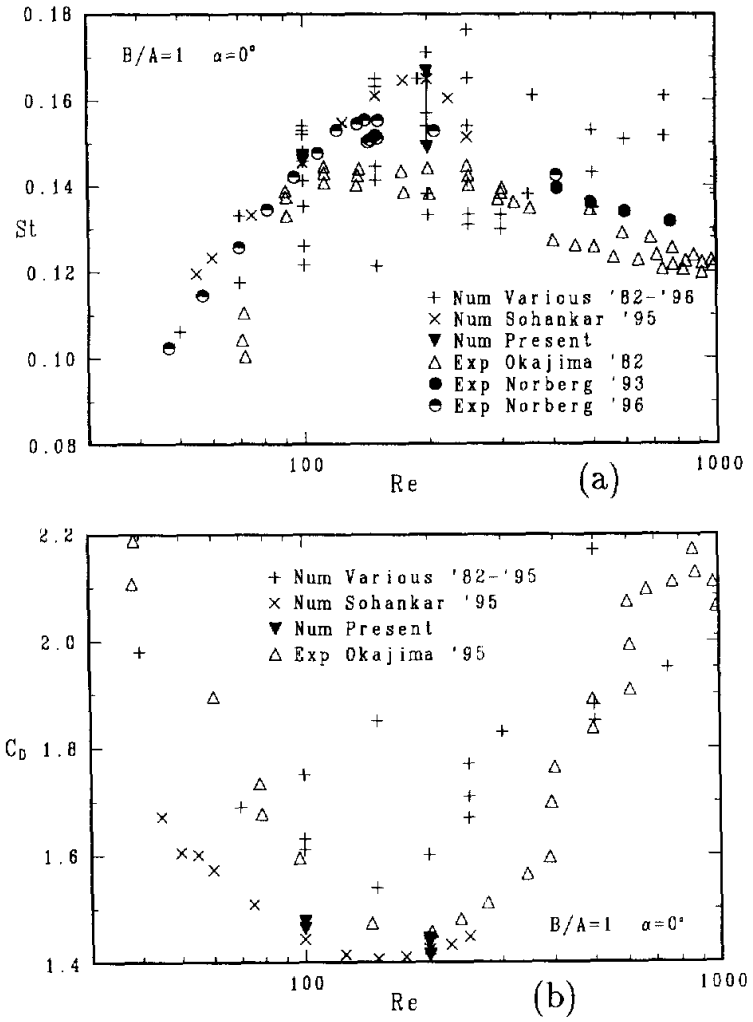

Fig. 2. Square cylinder at $\alpha = 0°$. (a) Strouhal number and (b) mean drag coefficient versus Re. Unpublished Strouhal number data of Norberg, 1996 ($d = 1.00$ mm, length-to-diameter $L/d = 200$, blockage 0.25%, measurements taken 30 diameters downstream).

reiterated that the present results as well as those in Ref. [15] are for a solid blockage of $\beta = 5\%$. Most other numerical results have higher blockages, e.g. $\beta = 8\%$ ($H = 12$–13) in Refs. [3,5,6,8,14]. For $Re \leqslant 200$ in Fig. 2 the experiments of Okajima et al. [14,17] are carried out at $\beta \leqslant 3.6\%$ (Okajima 1996, personal communication). At these low Re, as demonstrated in e.g. Refs. [22,15], the effect of an increase in β is to produce higher values in St and C_D. Considering these blockage effects, experimental uncertainties, different experimental conditions and effects due to various numerical factors, the agreement seems satisfactory. The recent experiments by Norberg, see Fig. 2a, indicated onset at $Re = 47 \pm 2$ and a transitional behaviour at $Re \simeq 150$ similar to the flow around a circular cylinder [23]. For the circular cylinder, by manipulating with the end conditions, the laminar shedding can be extended beyond $Re = 200$ for short periods of time [24]. The question whether an extension of the laminar regime beyond $Re = 200$ is possible also for the square cylinder needs further investigation.

Instantaneous and time-averaged pressure and vorticity fields in the fully developed state, for $Re = 100$ and 200, are shown in Fig. 3. Due to symmetry only flow instants during half a shedding period T are presented. With an equal time increment in the sequence, Fig. 3a, Fig. 3c and Fig. 3e, respectively, corresponds to zero (increasing), maximum and zero (decreasing) lift ($t'/T = 0$, 0.25, 0.5). Fig. 3f displays the time-averaged flow conditions. Resultant forces are shown by vectors while attachment and separation points are labelled A and S, respectively.

Previous numerical work by the authors [15] and later analysis show that the separation for $Re \leqslant 100$, at all times in the fully saturated state, occurred from the rear corners, predominantly from the rear corners at $Re = 125$ with occasional upstream corner separation, predominantly from upstream corners at $Re = 150$ and finally, at all times, from upstream corners for $Re \geqslant 175$. This is in reasonable agreement with Franke et al. [6], who reports separation from upstream corners for $Re > 150$ ($\beta = 8.3\%$). Further enlightenment on this fundamental change in the separation process is provided in Fig. 3.

At $t'/T = 0$ ($Re = 100$) a clockwise vortex is in development due to separation at the upper base corner, see Fig. 3a (left). As it grows, with increasing strength but being rather fixed in position, the attachment point on the base side is being pushed downwards, see Fig. 3a–c. As the attachment point more or less reaches the lower base corner, in between Fig. 3c and Fig. 3d, the lift already has passed its maximum level and a new anti-clockwise vortex is about to be formed at that lower base corner. As this new vortex grows, see Fig. 3d and Fig. 3e, the old clockwise vortex is being pushed away and is eventually shed into the wake. In general terms, the same trend occurs for $Re = 200$. The main difference between these two Reynolds numbers is that for $Re = 200$ separation instead occurs at the frontal corners which causes a reverse flow at the top and bottom of the body. Interestingly, for $Re = 200$ and at the instants of zero lift, Fig. 3a and Fig. 3e, the flow is actually very close to a reattachment at the base corner. At this Re, as discussed further in the next section, the necessary streamwise body length to produce a permanent reattachment is within 1.5 and 2 projected widths (length units).

Due to stronger vortex shedding the minimum time mean pressure along the base centerline is about 70% lower at $Re = 200$ compared to $Re = 100$. However, the

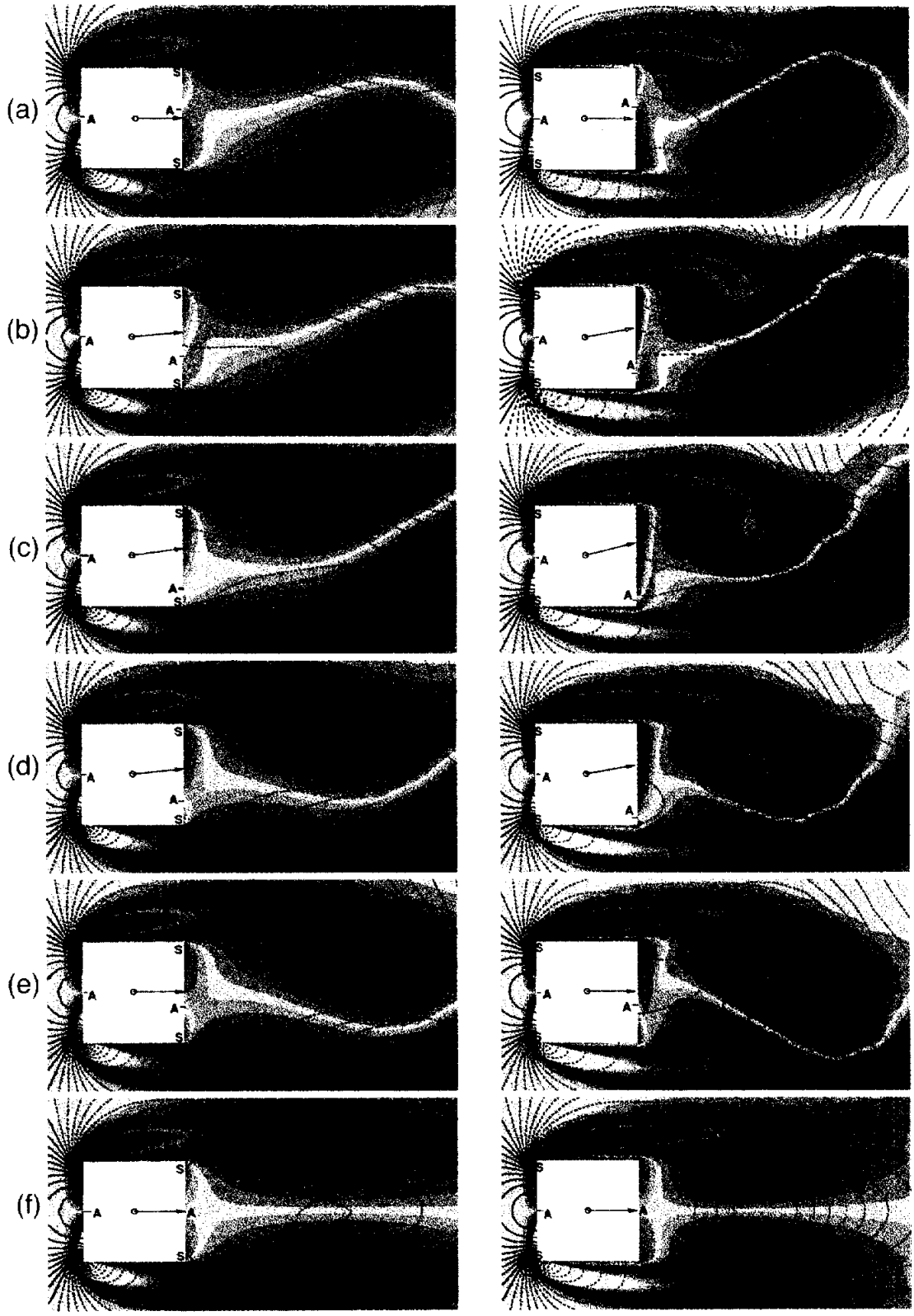

Fig. 3. Square cylinder at zero incidence. (a)–(e) Time sequence during half period of vortex shedding, (f) time-averaged flow. Iso-contours of pressure (solid lines: $C_p > 0$, dashed: $C_p < 0$, $\Delta C_p \simeq 0.1$) and color-coded vorticity (yellow corresponds to zero vorticity). Re = 100 (left), Re = 200 (right).

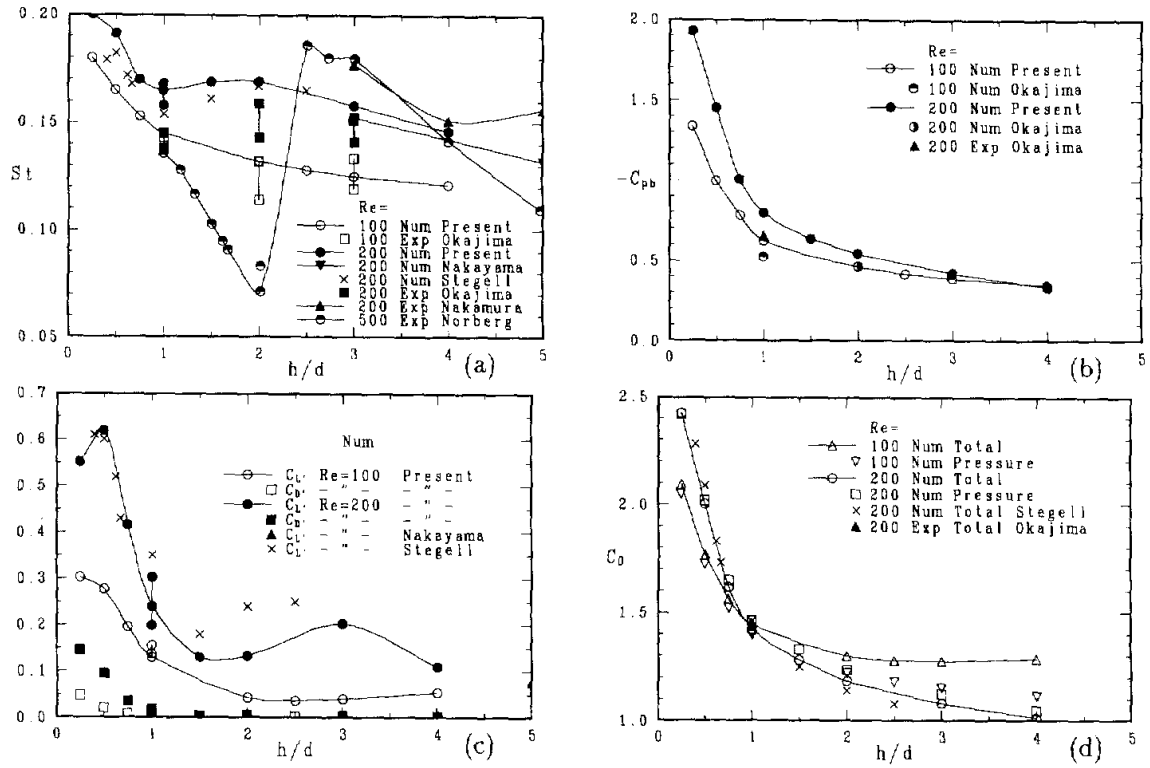

Fig. 4. (a) Strouhal number, (b) base suction coefficient, (c) RMS lift and drag coefficients, and (d) mean drag coefficients versus projected side ratio. Present results except refinement points: downstream $\Delta = 0.5$, other parts $\Delta = 0.7$.

position of this minimum pressure remains more or less fixed, see Fig. 3f. The mean wake closure point, for both Re being downstream of the point of minimum pressure, exhibited an upstream movement of 25% towards the base with increasing Re (at Re = 100 the closure point was 2.2 length units downstream of the base).

3.3. *Influence of projected side ratio ($\alpha = 0°$, 90°)*

In Fig. 4 the present data on various quantities versus projected side ratio h/d for Re = 100 and 200 are shown together with numerical data of Nakayama et al. [11] and Stegell and Rockliff [25] and experimental results as given by Okajima [4,17], Nakamura et al. [16] and Norberg [2]. For Re = 100 the Strouhal number (St) decreases smoothly by side ratio but for Re = 200 it increases rather abruptly at around $h/d = 1.5$. At $h/d \geqslant 2$ for Re = 200 the flow reattaches on the longest side which is not the case at $h/d < 2$. For Re = 100 at all side ratios investigated, separation points are located at the leeward corners, but for Re = 200, they are located at the windward corners with back-flow occurring at the side surface. Up to $h/d = 1$ this back flow covers the whole surface but by increasing the side ratio, attachment points appear at the side surfaces which causes a small jump in St, see Fig. 4a. At $h/d = 2$, these attachment points are located near to the leeward corners with subsequent separation. In terms of the diameter d, the reattachment lengths at

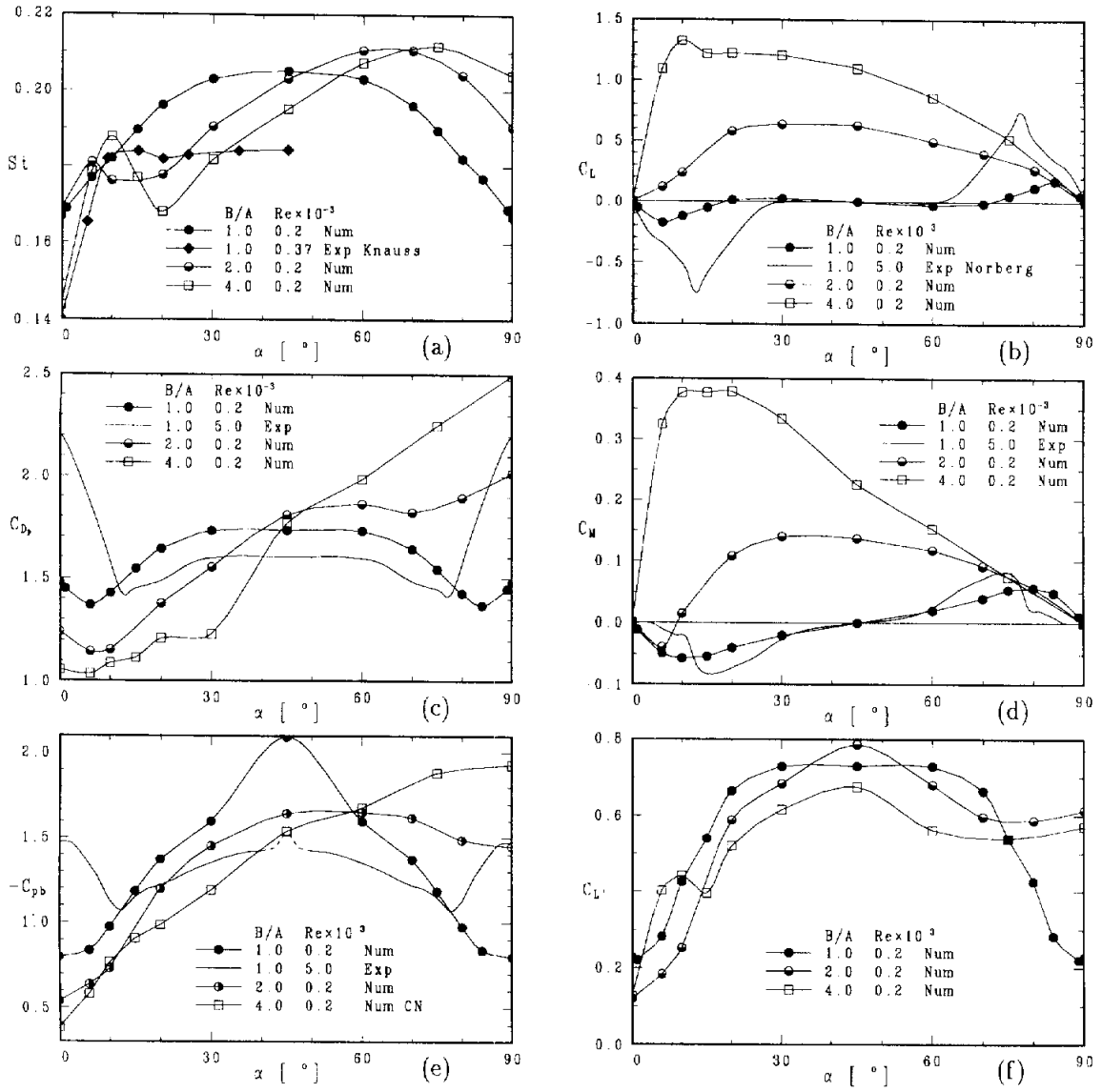

Fig. 5. (a) Strouhal number, (b) lift coefficient, (c) pressure drag coefficient, (d) moment coefficient, (e) base suction coefficient, and (f) RMS lift coefficient versus angle of incidence.

$h/d = 3$ and 4 are approximately the same as for $h/d = 2$. At $h/d = 1.5$ the mean flow is close to but not fully reattached. Thus the critical length for reattachment seems to be in between $h/d = 1.5$ and 2. At this Re = 200, in agreement with Ref. [25], there is no spectacular jump in St as found at higher Re in turbulent flow, see e.g. Re = 500 in Fig. 4a. For both Strouhal number and RMS lift, local extreme values were indicated at this critical length. The experiments in Ref. [16] indicate Re $\simeq$ 250 as the critical Re for the appearance of a jump in St. In their experiments, however, the emphasis was put on elongated cylinders with $h/d = 3$–16. Nevertheless, their Strouhal numbers at $h/d = 3$ and 4 are in good agreement with the present data, see Fig. 4a.

Interestingly, there was no indication of a local maximum in the drag coefficient or base suction coefficient at some intermediate critical side ratio, see Fig. 4d and

Fig. 4b. In turbulent flow, such a maximum occurs at around $h/d = 0.6$, see e.g. Refs. [1,2]. Obviously, this type of shear layer/edge interaction does not occur in laminar vortex shedding flow. The vortex shedding strength, as indicated from RMS coefficients in Fig. 4c, shows a drastic decrease with increasing h/d. For instance, at $\mathrm{Re} = 100$, the RMS lift coefficient at $h/d = 2$ is about 3 times lower than at $h/d = 1$.

It is worth noting that the present results show a good agreement with the recent data of Stegell and Rockliff [25]. They use a completely different numerical procedure (a hybrid discrete vortex method) at a fine resolution and with very large grid in the physical domain (Stegell, 1996, personal communication).

3.4. *Influence of angle of incidence*

At $\mathrm{Re} = 200$, an extensive investigation of the influence of the angle of incidence from 0° to 90° and at side ratios $B/A = 1,2,4$ was performed. The results for Strouhal number, pressure drag, base suction, mean lift, RMS lift and moment coefficients are shown in Fig. 5. For cases within the approx. ranges $0° \leqslant \alpha < 20°$ and $70 \leqslant \alpha \leqslant 90°$ the variation of these quantities exhibited a somewhat more complex behavior compared to cases at incidences in between. At $B/A > 1$, the complexity is biased towards the lower range of incidences and this is due to the presence of secondary separation occurring on the leeward (upper) side surface. For $\alpha \geqslant 6°$ the ordinary separation points were fixed at the two corners which define the projected side (Fig. 1). No separation was present on the windward sides.

With increasing angle of incidence from $\alpha = 0°$ there is an increase in the Strouhal number, see Fig. 5a. This may simply be due to an increase in the feeding velocity around the lower base corner. In addition, the change in position for the ordinary separation point from the upstream lower corner to the lower rear corner is affecting the shedding frequency. At some critical angle somewhere in between $\alpha = 6°$ and 10° ($B/A > 1$), St reaches a local maximum value. At around this critical angle, an anti-clockwise vortex forms somewhere on the downstream part of the leeward upper surface. The clockwise vortex which is fed by separation at the upper windward corner is controlled by this secondary vortex. The drop in St, e.g. in between $\alpha = 10°$ and 20° for $B/A = 4$, is believed to be due to the downstream movement of this secondary bubble slowing up the shedding process. At higher α, the bubble is still present but now it only appears fixed to the rear upper corner, the timing control from it vanishes and the Strouhal number increases again. In contrast to turbulent flow conditions [26,2], at intermediate angles i.e. approx. $20° < \alpha < 70°$, the Strouhal number does not collapse into a more or less constant value, see Fig. 5a. Evidently, the frequency scaling at laminar shedding conditions need further investigation.

About other quantities in Fig. 5, there are some similarities with turbulent flow conditions, as exemplified by the inserted experimental data at $B/A = 1$ for $\mathrm{Re} = 5 \times 10^3$ [14]. As in turbulent flow, when one side is facing the flow, the square cylinder has a stable posture, see Fig. 5d. Also as in turbulent flow [2], the square cylinder at $\alpha = 0°$ for $\mathrm{Re} = 200$ was found to be dynamically unstable with respect to quasi-steady galloping in the plunging mode. Interestingly, for $B/A = 4$, the present moment data indicated an unstable posture at $\alpha = 0°$, in contrast to turbulent flow.

4. Conclusions

Apart from the physical parameters investigated, i.e. Reynolds number, body side ratio and angle of incidence, it was found that the results also were strongly dependent on various numerical parameters such as time step, domain size and spatial resolution in both far and near field. Some of the discrepancies between present results and those from previous numerical studies have to be attributed to differences in the above-mentioned numerical parameters. When using the RMS lift coefficient as an indicator the strong sensitivity to various numerical parameters was demonstrated.

At $Re = 100$, for cases with one side opposing the flow, the flow separates at downstream corners. At $Re = 200$, however, the separation occurs at upstream corners with fully attached separation bubbles present at projected body ratios $h/d \geqslant 2$. The change to this reattached flow occurs in between $h/d = 1.5$ and 2.

The behavior of all quantities at low angles of incidence (approx. $\alpha < 20^\circ$) and at high angles (approx. $\alpha > 70^\circ$) is significantly different from that between these regions. This is due to fundamentally different evolutions of flow features close to the cylinder.

References

[1] P.W. Bearman, D.M. Trueman, Aeronautical Quart. 23 (1972) 229–237.
[2] C. Norberg, J. Wind Eng. Ind. Aerodyn. 49 (1993) 187–196.
[3] R.W. Davis, E.F. Moore, J. Fluid Mech. 116 (1982) 475–506.
[4] A. Okajima, J. Fluid Mech. 123 (1982) 379–398.
[5] R.W. Davis, E.F. Moore, L.P. Purtell, Phys. Fluids 27 (1) (1984) 46–59.
[6] R. Franke, W. Rodi, B. Schönung, J. Wind Eng. Ind. Aerodoyn. 35 (1990) 237–257.
[7] A. Okajima, T. Nagahisa, A. Rokugoh, JSME Int. J. Ser. II 33 (4) (1990) 702–711.
[8] M.P. Arnal, J.A.C. Goering, D.J. Humphrey, Trans. ASME: J. Fluids Eng. 113 (1991) 384–398.
[9] K.M. Kelkar, S.V. Patankar, Int. J. Num. Meth. Fluids 14 (3) (1992) 327–341.
[10] H. Suzuki, Y. Inoue, Int. J. Heat Fluid Flow 14 (1) (1993) 2–9.
[11] R. Nakayama, Y. Nakamura, Y. Ohya, S. Ozono, J. Wind Eng. Ind. Aerodyn. 46 (1993) 255–264.
[12] T. Yoshida, T. Watanabe, I. Nakamura, Trans. JSME 59 (565) (1993) 2799–2806; Paper No. 93-0270 (in Japanese).
[13] T.G. Zaki, M. Sen, M. Gad-El-Hak, J. Fluids Struct. 8 (1994) 555–582.
[14] G. Li, J.A.C. Humphrey, Int. J. Num. Meth. Fluids 20 (1995) 1215–1236.
[15] A. Sohankar, L. Davidson, C. Norberg, in: 12th Australasian Fluid Mech. Conf., Sydney, Australia, 10–15 December 1995, pp. 517–520.
[16] Y. Nakamura, Y. Ohya, S. Ozono, R. Nakayama, J. Wind Eng. Ind. Aerodyn. 65 (1996) 301–308.
[17] A. Okajima, in: Proc. 6th Int. Conf. Flow-Induced Vibration, London, UK, 10–12 April 1995, pp. 1–7.
[18] A. Sohankar, C. Norberg, L. Davidson, Report N. 96/25, Dept. Thermo and Fluid Dynamics, Chalmers University of Technology, Gothenburg, Sweden, May 1996.
[19] G.E. Karniadakis, Trans. ASME: J. Fluids Eng. 117 (1995) 7–9.
[20] A. Sohankar, C. Norberg, L. Davidson, Report, Dept. Thermo and Fluid Dynamics, Chalmers University of Technology, Sweden, October 1996, to appear in Int. J. Num. Meth. Fluids (1997).
[21] J.R. Manson, G. Pender, S.G. Wallis, AIAA J. 34 (5) (1996) 1074–1076.

[22] M. Behr, D. Hastreiter, S. Mittal, T.E. Tezduyar, Comput. Meth. Appl. Mech. Eng. 123 (1995) 309–316.
[23] C. Norberg, J. Fluid Mech. 258 (1994) 287–316.
[24] C.H.K. Williamson, Annual Rev. Fluid Mech. 28 (1996) 477–539.
[25] N. Stegell, N. Rockliff, in: H. W. Tieleman, M. Hajj, (Eds.), Proc. 3rd Int. Coll. Bluff-Body Aerodynamics & Applications (BBAA III), Blacksburg, VA, 1996; These Proceedings, J. Wind Eng. Ind. Aerodyn. 69–71 (1997) 317–329.
[26] D.T. Knauss, J.E.A. John, C.H. Marks, J. Hydronautics 10 (4) (1976) 121–126.